• RESEARCH PAPER •

Performance evaluation for underlay cognitive satellite-terrestrial cooperative networks

Yuhan RUAN[1], Yongzhao LI[1*], Cheng-Xiang WANG[2],
Rui ZHANG[1] & Hailin ZHANG[1]

[1]*State Key Laboratory of Integrated Service Network, Xidian University, Xi'an 710071, China;*
[2]*School of Engineering and Physical Sciences, Heriot-Watt University, Edinburgh EH14 4AS, UK*

Abstract With the continuously increasing demand for broadband applications and services, underlay cognitive satellite-terrestrial networks, enabling to accommodate better wireless services within the scarce spectrum, have attracted tremendous attentions recently. In this network, satellite communications are allowed to operate in the frequency bands allocated to terrestrial networks under the interference constraints imposed by terrestrial network, which may lead to a performance degradation of the satellite network. To guarantee the performance of the primary terrestrial network as well as the secondary satellite network, we introduce the cooperation into cognitive satellite-terrestrial networks and investigate the performance of the new framework, i.e., cognitive satellite-terrestrial cooperative network (CSTCN). Specifically, by restricting the transmit power of satellite communications with interference power constraints imposed by terrestrial communications, we firstly obtain the received signal-to-interference-plus-noise ratio (SINR) of the considered network. Moreover, by employing the moment generating function (MGF) approach, closed-form expressions for symbol error rate (SER) and outage probability (OP) of the considered cognitive network are derived. The analytical results obtained in this paper can provide theoretical support for optimizing the performance of satellite-terrestrial networks.

Keywords cognitive satellite-terrestrial cooperative network, interference constraints, moment generating function, symbol error rate, outage probability

1 Introduction

With the potential to realize genuine ubiquitous communication, the hybrid satellite-terrestrial network (HSTN) is becoming one of the most promising infrastructures for next generation communications [1–3]. In this context, the performance of the HSTN has been widely investigated in the open literatures. The authors in [4] analyzed the capacity upper bound of the HSTN, while a fundamental tradeoff between spectral efficiency and energy efficiency was studied in [5]. Extension work to multi-antenna satellite communications can be found in [6,7]. In [6], the authors investigated the symbol error rate (SER) and the average capacity of the orthogonal space-time block coding (OSTBC) based transmission over the shadowed-Rician fading. To retain the benefits of onboard beamforming and reduce the complexity of adaptive processing, the authors in [7] proposed a semi-adaptive beamformer for the HSTN.

---

* Corresponding author (email: yzhli@xidian.edu.cn)

However, the limited spectral resources cannot satisfy the increasing demand for broadband applications in satellite communications [8] as well as fifth-generation (5G) communications [9,10]. Accordingly, cognitive radio technology has arisen as a promising approach to cope with the problems of spectrum shortage and underutilization in satellite-terrestrial systems [11]. Regarding to the spectrum access policy, the cognitive satellite-terrestrial systems can operate on underlay, overlay, or interweave mode [12]. The underlay mode has drawn increasing attentions due to its highest spectral efficiency, which allows the secondary users to access the spectrum licensed to primary users without violating the interference constraints [13]. In this scenario, the authors in [14] evaluated the interference between terrestrial and satellite systems using a joint interference-noise estimation algorithm. The authors in [15] adopted the concept of exclusion region to protect the satellite transmission. Taking the inter-system and intra-system interference into account, the authors in [16] analyzed the outage performance of the terrestrial communication. To maximize the satellite throughput, the authors introduced a carrier-power-bandwidth allocation scheme and a game-theory based scheduling algorithm in [17,18], respectively.

Although coexisting with the primary system in the underlay mode can increase the system spectral efficiency, the secondary system has to carefully control its transmit power to avert excessive interference to primary receivers, which leads to a performance degradation of the secondary network. Moreover, in the satellite communication with shadowing effect, occurring when the line-of-sight (LOS) link is obstructed by obstacles, the mobile user will suffer a poor performance. To tackle this concern, based on the observation in [19], it is meaningful to introduce cooperative relaying in cognitive satellite-terrestrial networks as a promising candidate to enhance the performance of secondary systems without increasing the transmit power. In this context, only the authors in [20] theoretically analyzed the outage performance of a cognitive satellite-terrestrial relay network working in decode-and-forward protocol, while the direct link from satellite to destination was not considered. Until now, cooperative transmission with direct link has only been employed in HSTNs without cognitive radio [21–23]. By adopting maximal ratio combining (MRC) at the destination, the authors in [21,22] evaluated the SER performance of an amplify-and-forward (AF) based hybrid satellite-terrestrial cooperative networks, while the authors in [23] adopted the distributed space-time code into the hybrid satellite-terrestrial cooperative network to achieve transmit diversity and conducted the SER performance analysis. These studies verified that in satellite-terrestrial networks, employing cooperation can exploit the advantage of spatial diversity, thus improving the performance of satellite-terrestrial networks. To the best of our knowledge, the performance analysis for the cognitive satellite-terrestrial network employing cooperation is still missing in the literature.

To fill this research gap, an AF based cognitive satellite-terrestrial cooperative network (CSTCN) is introduced and investigated in this paper for the first time. In the considered network, the terrestrial network is regarded as the primary system and the satellite network operates as the secondary system. By restricting the transmit power of satellite communications with interference power constraints imposed by terrestrial communications and applying MRC at the destination, we firstly derive the received signal-to-interference-plus-noise ratio (SINR) of the CSTCN. Moreover, by using the moment generating function (MGF) approach, closed-form expressions for SER and outage probability (OP) of the considered CSTCN are obtained, providing insights into the impacts of various system parameters, for example, interference threshold, fading condition of satellite and terrestrial links, on the performance of the considered network.

The remainder of the paper is organized as follows. Section 2 introduces the signal model and the channel model. Section 3 numerically evaluates SER and OP performance for the CSTCN. Simulations and analysis are given in Section 4. Finally, Section 5 concludes this paper.

2 System model

As illustrated in Figure 1, we consider an AF based CSTCN, where the satellite (S) transmits signals to the destination (D) with the aid of the terrestrial relay (R) exploiting the spectrum bands allocated to the terrestrial cellular network. In this case, S and R will interfere the cellular receiver (C) while R and
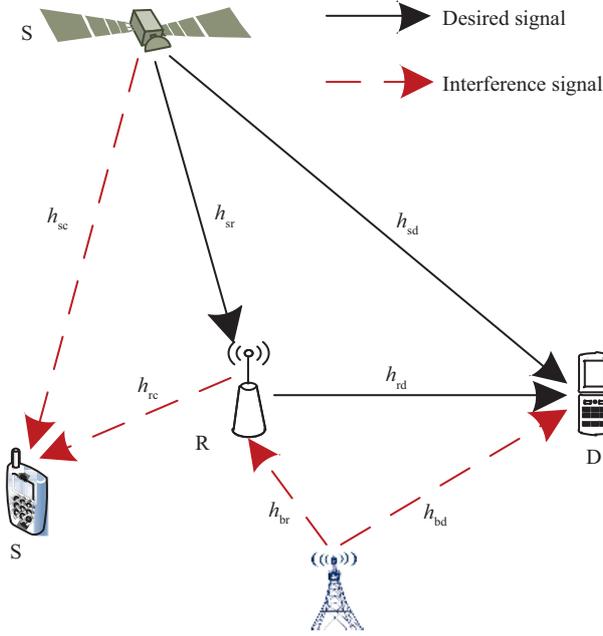
Figure 1 (Color online) System model of the underlaying CSTCN.

D will also suffer from the interference caused by the base station (BS). Each node is equipped with a single antenna. We denote h_{sr}, h_{sd}, and h_{rd} as the channel coefficients of S $\rightarrow$ R, S $\rightarrow$ D, and R $\rightarrow$ D communication links, respectively, while h_{sc}, h_{rc}, h_{br}, and h_{bd} as the channel coefficients of S $\rightarrow$ C, R $\rightarrow$ C, BS $\rightarrow$ R, and BS $\rightarrow$ D interfering links, respectively.

2.1 Signal model

The transmission of the satellite communication occurs during two time phases. During the first phase, the S broadcasts its signal to the R and D with power P_s. The received signals at R and D can be respectively written as

$$y_{sr} = \sqrt{P_s}\, h_{sr}\, x + \sqrt{P_b}\, h_{br}\, z + n_{sr}, \tag{1}$$

and

$$y_{sd} = \sqrt{P_s}\, h_{sd}\, x + \sqrt{P_b}\, h_{bd}\, z + n_{sd}, \tag{2}$$

where P_b denotes the transmit power of the BS, n_{sr} and n_{sd} are the noises at R and D in the first phase, respectively. It is assumed that all the noises in this paper are complex additive white Gaussian noises (AWGNs) each with power N_0. After receiving signals from the satellite, the relay multiplies the received signal y_{sr} with a factor ρ. Here, $\rho = 1/\sqrt{P_s|h_{sr}|^2 + P_b|h_{br}|^2 + N_0}$. Then, the relay forwards the amplified signal to the destination with transmit power P_r, yields

$$y_{rd} = \sqrt{P_r}\, h_{rd}\, \rho\, y_{sr} + \sqrt{P_b}\, h_{bd}\, z + n_{rd}, \tag{3}$$

where n_{rd} is the noise at the destination in the second phase.

By assuming MRC employed at the destination, we have the instantaneous SINR for the satellite communication as

$$\gamma_{\text{coop}} = \gamma_{sd} + \gamma_{srd}, \tag{4}$$

where γ_{sd} and γ_{srd} are the SINRs for the S-D link and the S-R-D link, respectively.

In the considered network, to prevent the primary cellular communication from being interfered seriously, we guarantee the interference received at the cellular receiver remains below a predefined threshold I_{th}. In this case, the transmit power at the satellite and the relay can be, respectively, given by

$P_{\rm s} = I_{\rm th}/|h_{\rm sc}|^2$ and $P_{\rm r} = I_{\rm th}/|h_{\rm rc}|^2$. Then, $\gamma_{\rm sd}$ can be expressed as

$$\gamma_{\rm sd} = \frac{\frac{I_{\rm th}}{|h_{\rm sc}|^2}|h_{\rm sd}|^2}{P_{\rm b}|h_{\rm bd}|^2 + N_0} = \frac{\bar{\gamma}_{\rm th}\frac{|h_{\rm sd}|^2}{|h_{\rm sc}|^2}}{\bar{\gamma}_{\rm b}|h_{\rm bd}|^2 + 1}, \tag{5}$$

where $\bar{\gamma}_{\rm th} = I_{\rm th}/N_0$ and $\bar{\gamma}_{\rm b} = P_{\rm b}/N_0$. From (3), $\gamma_{\rm srd}$ can be expressed as

$$\gamma_{\rm srd} = \frac{UV}{U + V + 1}, \tag{6}$$

where $U = \frac{\frac{I_{\rm th}}{|h_{\rm sc}|^2}|h_{\rm sr}|^2}{P_{\rm b}|h_{\rm br}|^2 + N_0} = \frac{\bar{\gamma}_{\rm th}\frac{|h_{\rm sr}|^2}{|h_{\rm sc}|^2}}{\bar{\gamma}_{\rm b}|h_{\rm br}|^2 + 1}$ and $V = \frac{\frac{I_{\rm th}}{|h_{\rm rc}|^2}|h_{\rm rd}|^2}{P_{\rm b}|h_{\rm bd}|^2 + N_0} = \frac{\bar{\gamma}_{\rm th}\frac{|h_{\rm rd}|^2}{|h_{\rm rc}|^2}}{\bar{\gamma}_{\rm b}|h_{\rm bd}|^2 + 1}$.

2.2 Channel model

2.2.1 *Satellite links*

The most popular land mobile satellite (LMS) model is the Loo model [24], where the power of the LOS component obeys log-normal distribution and the multipath component follows Rayleigh distribution. Due to the existence of log-normal distribution, it is usually analytically intractable when adopting the Loo channel model. In this paper, we employ the widely used generalized-K distribution to characterize a composite multipath/shadowing fading environment because of its relatively simple mathematical form. In the generalized-K distribution, the shadowing fading is gamma-distributed while the multipath fading is Nakagami-distributed. As illustrated in [25,26], the generalized-K model can properly characterize the satellite channel environment.

For the generalized-K model, the probability density function (PDF) of $|h_i|^2$ ($i = {\rm sr}, {\rm sd}, {\rm sc}$) can be written as

$$f_{|h_i|^2}(x) = \frac{2b_i^{\varphi_i + \varepsilon_i}}{\Gamma(\varepsilon_i)\Gamma(\varphi_i)}x^{\left(\frac{\varphi_i + \varepsilon_i}{2}\right) - 1}K_{\varphi_i - \varepsilon_i}(2b_i\sqrt{x}), \ x > 0, \ \varepsilon_i \geqslant 0.5, \ \varphi_i \geqslant 0, \tag{7}$$

where $K_{\varphi_i - \varepsilon_i}(\cdot)$ denotes the modified Bessel function of the second kind with order $(\varphi_i - \varepsilon_i)$, $b_i = \sqrt{\frac{\varphi_i \varepsilon_i}{\Omega_i}}$, ε_i and φ_i are the multipath and shadowing parameters, respectively, Ω_i is the mean of the received local power.

2.2.2 *Terrestrial links*

Terrestrial links h_j ($j = {\rm rd}, {\rm rc}, {\rm br}, {\rm bd}$) is modeled as the Nakagami-m fading channel, the PDF of the channel power gain can be expressed as

$$f_{|h_j|^2}(x) = \frac{m_j^{m_j}x^{m_j - 1}}{\Gamma(m_j)\Omega_j^{m_j}}{\rm e}^{-\frac{m_j x}{\Omega_j}}, \tag{8}$$

where $m_j \geqslant 0.5$ represents the fading parameter of Nakagami-m distribution, Ω_j is the average power, $\Gamma(n) = \int_0^\infty x^{n-1}{\rm e}^{-x}{\rm d}x$ denotes the Gamma function, and $\Gamma(n) = (n-1)!$ when n takes integer values [27, Eq. (8.310.1)].

3 Performance analysis for the underlay CSTCN

In this section, we investigate the SER and OP performance for the considered CSTCN. Considering in cooperative communications, traditional PDF based SER/OP derivation is intractable, we employ the MGF approach to analyze the related performance. Specifically, we first introduce the MGF based SER and OP definition, which converts the intractable statistical derivation of cooperation with three communication links to a new tractable problem consisting of statistical derivations of the S-D link and S-R-D link. Then, according to the existing theoretical framework, we derive the analytical expressions of the cumulative distribution functions (CDFs) and MGFs of $\gamma_{\rm sd}$ and $\gamma_{\rm srd}$, respectively. Based on these statistical properties, we finally obtain closed-form expressions for the SER and OP.

3.1 MGF based SER and OP evaluation

According to [28], the SER of a wireless system with M-ary phase-shift keying (MPSK) modulation can be expressed as

$$\mathcal{P}_{\mathrm{ser}} = \frac{1}{\pi} \int_0^{\theta_M} M_{\gamma_{\mathrm{coop}}} \left(\frac{g_{M\mathrm{PSK}}}{\sin^2\theta} \right) \mathrm{d}\theta, \tag{9}$$

where $\theta_M = \pi(M-1)/M$ and $g_{M\mathrm{PSK}} = \sin^2(\pi/M)$.

In the AF-based CSTCN where direct link exists, it is mathematically intractable to obtain a closed-form expression for the OP through the PDF-based approach. Thus, in this paper, we employ a novel MGF-based method to analyze the OP, $\mathcal{P}_{\mathrm{out}}$, which can be written as [29]

$$\mathcal{P}_{\mathrm{out}} = \frac{2^{-M}\mathrm{e}^{-\frac{B}{2}}}{\Theta_{\mathrm{th}}} \sum_{m=0}^{M} \binom{M}{m} \sum_{n=0}^{N+m} \frac{(-1)^n}{\theta_n} \mathrm{Re} \left\{ \frac{M_{\gamma_{\mathrm{coop}}} \left(\frac{B+\mathrm{j}2\pi n}{2\Theta_{\mathrm{th}}} \right)}{\frac{B+\mathrm{j}2\pi n}{2\Theta_{\mathrm{th}}}} \right\}, \tag{10}$$

where $\mathrm{Re}\{\cdot\}$ means the real part of a complex number, Θ_{th} is the threshold of the received SINR, $B = 23.06$, $N = 15$, $M = 21$, $\theta_n = 2$ for $n = 0$, and $\theta_n = 1$ for $n = 1, 2, \ldots$ [29].

From (9) and (10) we can see that, to derive the closed-form expressions for both SER and OP, we need to derive $M_{\gamma_{\mathrm{coop}}}(s)$ firstly.

To make the subsequent derivation tractable, we employ the CDF based MGF definition. In this way, the MGF of a random variable can be expressed as [26]

$$M_\gamma(s) = \int_0^\infty s\mathrm{e}^{-s\gamma} F_\gamma(\gamma) \mathrm{d}\gamma. \tag{11}$$

From (11) we observe the MGF of the sum of two independent variables can be calculated by the product of their own MGFs. Thus, for the received SINR $\gamma_{\mathrm{coop}} = \gamma_{\mathrm{sd}} + \gamma_{\mathrm{srd}}$, we can express $M_{\gamma_{\mathrm{coop}}}(s)$ as

$$M_{\gamma_{\mathrm{coop}}}(s) = M_{\gamma_{\mathrm{sd}}}(s) M_{\gamma_{\mathrm{srd}}}(s), \tag{12}$$

where $M_{\gamma_{\mathrm{sd}}}(s)$ and $M_{\gamma_{\mathrm{srd}}}(s)$ are the MGFs of γ_{sd} and γ_{srd}, respectively. It can be observed from (12) that $M_{\gamma_{\mathrm{coop}}}(s)$ depends on $M_{\gamma_{\mathrm{sd}}}(s)$ and $M_{\gamma_{\mathrm{srd}}}(s)$. Thus, we focus on deriving $M_{\gamma_{\mathrm{sd}}}(s)$ and $M_{\gamma_{\mathrm{srd}}}(s)$ in the subsections.

3.2 Derivation of $M_{\gamma_{\mathrm{sd}}}(s)$

For direct link, the SINR γ_{sd} specified in (5) can be written as $\gamma_{\mathrm{sd}} = \frac{\bar{\gamma}_{\mathrm{th}} X}{\bar{\gamma}_{\mathrm{b}}|h_{\mathrm{bd}}|^2+1}$ with $X = \frac{|h_{\mathrm{sd}}|^2}{|h_{\mathrm{sc}}|^2}$. Then, we can get the PDF of γ_{sd} as

$$f_{\gamma_{\mathrm{sd}}}(x) = \int_0^\infty \frac{y}{\bar{\gamma}_{\mathrm{th}}} f_{\bar{\gamma}_{\mathrm{b}}|h_{\mathrm{bd}}|^2}(y) f_X\left(\frac{xy}{\bar{\gamma}_{\mathrm{th}}}\right) \mathrm{d}y. \tag{13}$$

We first calculate $f_X(x)$ through

$$f_X(x) = \int_0^\infty y f_{|h_{\mathrm{sc}}|^2}(y) f_{|h_{\mathrm{sd}}|^2}(xy) \mathrm{d}y. \tag{14}$$

By substituting (7) into (14), we can get

$$f_X(x) = \frac{4b_{\mathrm{sc}}^{\varphi_{\mathrm{sc}}+\varepsilon_{\mathrm{sc}}} b_{\mathrm{sd}}^{\varphi_{\mathrm{sd}}+\varepsilon_{\mathrm{sd}}}}{Q_1} x^{\tilde{\varphi}_{\mathrm{sd}}-1} \int_0^\infty y^{\tilde{\varphi}_{\mathrm{sc}}+\tilde{\varphi}_{\mathrm{sd}}-1} K_{\varphi_{\mathrm{sc}}-\varepsilon_{\mathrm{sc}}}\left(2b_{\mathrm{sc}}\sqrt{y}\right) K_{\varphi_{\mathrm{sd}}-\varepsilon_{\mathrm{sd}}}\left(2b_{\mathrm{sd}}\sqrt{xy}\right) \mathrm{d}y, \tag{15}$$

where $Q_1 = \Gamma(\varepsilon_{\mathrm{sc}})\Gamma(\varphi_{\mathrm{sc}})\Gamma(\varepsilon_{\mathrm{sd}})\Gamma(\varphi_{\mathrm{sd}})$, $\tilde{\varphi}_{\mathrm{sc}} = \frac{\varphi_{\mathrm{sc}}+\varepsilon_{\mathrm{sc}}}{2}$, $\tilde{\varepsilon}_{\mathrm{sc}} = \frac{\varphi_{\mathrm{sc}}-\varepsilon_{\mathrm{sc}}}{2}$, $\tilde{\varphi}_{\mathrm{sd}} = \frac{\varphi_{\mathrm{sd}}+\varepsilon_{\mathrm{sd}}}{2}$, and $\tilde{\varepsilon}_{\mathrm{sd}} = \frac{\varphi_{\mathrm{sd}}-\varepsilon_{\mathrm{sd}}}{2}$. To derive this integral, we express the $K_{\varphi_i-\varepsilon_i}(\cdot)$ functions into Meijer-G functions as [30, Eq. (14)]

$$K_{\varphi_{\mathrm{sc}}-\varepsilon_{\mathrm{sc}}}\left(2b_{\mathrm{sc}}\sqrt{y}\right) = \frac{1}{2} G_{02}^{20} \left[b_{\mathrm{sc}}^2 y \,\middle|\, \begin{matrix} - \\ \tilde{\varepsilon}_{\mathrm{sc}}, -\tilde{\varepsilon}_{\mathrm{sc}} \end{matrix} \right], \tag{16}$$

and

$$K_{\varphi_{\mathrm{sd}}-\varepsilon_{\mathrm{sd}}}\left(2b_{\mathrm{sd}}\sqrt{xy}\right)=\frac{1}{2}G_{02}^{20}\left[b_{\mathrm{sd}}^2 xy\,\middle|\,\begin{array}{c} - \\ \tilde{\varepsilon}_{\mathrm{sd}},-\tilde{\varepsilon}_{\mathrm{sd}} \end{array}\right].\tag{17}$$

With the aid of [27, Eq. (7.811.1)], Eq. (15) can be obtained as

$$f_X\left(x\right)=\frac{x^{\tilde{\varphi}_{\mathrm{sd}}-1}}{Q_1}G_{22}^{22}\left[\frac{b_{\mathrm{sd}}^2}{b_{\mathrm{sc}}^2}x\,\middle|\,\begin{array}{c} 1-\varphi_{\mathrm{sc}}-\tilde{\varphi}_{\mathrm{sd}},1-\varepsilon_{\mathrm{sc}}-\tilde{\varphi}_{\mathrm{sd}} \\ \tilde{\varepsilon}_{\mathrm{sd}},-\tilde{\varepsilon}_{\mathrm{sd}} \end{array}\right].\tag{18}$$

Then, substituting (8) and (18) into (13), $f_{\gamma_{\mathrm{sd}}}(x)$ can be given by

$$f_{\gamma_{\mathrm{sd}}}\left(x\right)=\frac{m_{\mathrm{bd}}^{m_{\mathrm{bd}}}x^{\tilde{\varphi}_{\mathrm{sd}}-1}}{\Gamma(m_{\mathrm{bd}})Q_1(\bar{\gamma}_{\mathrm{b}}\Omega_{\mathrm{bd}})^{m_{\mathrm{bd}}}\bar{\gamma}_{\mathrm{th}}^{\tilde{\varphi}_{\mathrm{sd}}}}\int_0^\infty y^{m_{\mathrm{bd}}+\tilde{\varphi}_{\mathrm{sd}}-1}\mathrm{e}^{-\frac{m_{\mathrm{bd}}}{\bar{\gamma}_{\mathrm{b}}\Omega_{\mathrm{bd}}}y}G_{22}^{22}\left[\frac{b_{\mathrm{sd}}^2 x}{\bar{\gamma}_{\mathrm{th}}b_{\mathrm{sc}}^2}y\,\middle|\,\begin{array}{c} 1-\varphi_{\mathrm{sc}}-\tilde{\varphi}_{\mathrm{sd}},1-\varepsilon_{\mathrm{sc}}-\tilde{\varphi}_{\mathrm{sd}} \\ \tilde{\varepsilon}_{\mathrm{sd}},-\tilde{\varepsilon}_{\mathrm{sd}} \end{array}\right]\mathrm{d}y.\tag{19}$$

According to [27, Eq. (7.813.1)], we can calculate (19) as

$$f_{\gamma_{\mathrm{sd}}}\left(x\right)=\frac{\left(\frac{\bar{\gamma}_b\Omega_{\mathrm{bd}}}{m_{\mathrm{bd}}\bar{\gamma}_{\mathrm{th}}}\right)^{\tilde{\varphi}_{\mathrm{sd}}}x^{\tilde{\varphi}_{\mathrm{sd}}-1}}{\Gamma\left(m_{\mathrm{bd}}\right)Q_1}G_{32}^{23}\left[\frac{b_{\mathrm{sd}}^2\bar{\gamma}_{\mathrm{b}}\Omega_{\mathrm{bd}}}{\bar{\gamma}_{\mathrm{th}}b_{\mathrm{sc}}^2 m_{\mathrm{bd}}}x\,\middle|\,\begin{array}{c} 1-m_{\mathrm{bd}}-\tilde{\varphi}_{\mathrm{sd}},1-\varphi_{\mathrm{sc}}-\tilde{\varphi}_{\mathrm{sd}},1-\varepsilon_{\mathrm{sc}}-\tilde{\varphi}_{\mathrm{sd}} \\ \tilde{\varepsilon}_{\mathrm{sd}},-\tilde{\varepsilon}_{\mathrm{sd}} \end{array}\right].\tag{20}$$

Then, from the definition of CDF and the identity in [30, Eq. (26)], we can derive the CDF of γ_{sd} as

$$F_{\gamma_{\mathrm{sd}}}(x)=\frac{\left(\frac{\bar{\gamma}_b\Omega_{\mathrm{bd}}}{m_{\mathrm{bd}}\bar{\gamma}_{\mathrm{th}}}\right)^{\tilde{\varphi}_{\mathrm{sd}}}}{\Gamma\left(m_{\mathrm{bd}}\right)Q_1}x^{\tilde{\varphi}_{\mathrm{sd}}}G_{43}^{24}\left[\frac{b_{\mathrm{sd}}^2\bar{\gamma}_{\mathrm{b}}\Omega_{\mathrm{bd}}}{\bar{\gamma}_{\mathrm{th}}b_{\mathrm{sc}}^2 m_{\mathrm{bd}}}x\,\middle|\,\begin{array}{c} 1-\tilde{\varphi}_{\mathrm{sd}},1-m_{\mathrm{bd}}-\tilde{\varphi}_{\mathrm{sd}},1-\varphi_{\mathrm{sc}}-\tilde{\varphi}_{\mathrm{sd}},1-\varepsilon_{\mathrm{sc}}-\tilde{\varphi}_{\mathrm{sd}} \\ \tilde{\varepsilon}_{\mathrm{sd}},-\tilde{\varepsilon}_{\mathrm{sd}},-\tilde{\varphi}_{\mathrm{sd}} \end{array}\right].\tag{21}$$

Finally, by substituting (21) into (11) and employing the equality in [27, Eq. (7.813.1)], we can obtain $M_{\gamma_{\mathrm{sd}}}\left(s\right)$ as

$$M_{\gamma_{\mathrm{sd}}}\left(s\right)=\frac{\left(\frac{\bar{\gamma}_b\Omega_{\mathrm{bd}}}{m_{\mathrm{bd}}\bar{\gamma}_{\mathrm{th}}}\right)^{\tilde{\varphi}_{\mathrm{sd}}}}{\Gamma\left(m_{\mathrm{bd}}\right)Q_1}s^{-\tilde{\varphi}_{\mathrm{sd}}}G_{42}^{24}\left[\frac{b_{\mathrm{sd}}^2\bar{\gamma}_{\mathrm{b}}\Omega_{\mathrm{bd}}}{s\bar{\gamma}_{\mathrm{th}}b_{\mathrm{sc}}^2 m_{\mathrm{bd}}}\,\middle|\,\begin{array}{c} 1-\tilde{\varphi}_{\mathrm{sd}},1-m_{\mathrm{bd}}-\tilde{\varphi}_{\mathrm{sd}},1-\varphi_{\mathrm{sc}}-\tilde{\varphi}_{\mathrm{sd}},1-\varepsilon_{\mathrm{sc}}-\tilde{\varphi}_{\mathrm{sd}} \\ \tilde{\varepsilon}_{\mathrm{sd}},-\tilde{\varepsilon}_{\mathrm{sd}} \end{array}\right].\tag{22}$$

Until now, we have derived the expression of $F_{\gamma_{\mathrm{sd}}}(x)$ and $M_{\gamma_{\mathrm{sd}}}(s)$, shown in (21) and (22).

3.3 Derivation of $M_{\gamma_{\mathrm{srd}}}(s)$

Considering the CDF of γ_{srd} specified in (6) is mathematically intractable, we employ the upper bound of the received SINR in (6) as $\gamma_{\mathrm{srd}}\leqslant\gamma_{\mathrm{srd}}^{\mathrm{up}}=\min(U,V)$ [31]. Then, we can get

$$F_{\gamma_{\mathrm{srd}}}\left(x\right)=1-\left[1-F_U\left(x\right)\right]\left[1-F_V\left(x\right)\right]=F_U\left(x\right)+F_V\left(x\right)-F_U\left(x\right)F_V(x).\tag{23}$$

As a result, $M_{\gamma_{\mathrm{srd}}}(s)$ can be expressed as

$$M_{\gamma_{\mathrm{srd}}}\left(s\right)=M_U(s)+M_V(s)-M_{UV}(s),\tag{24}$$

where $M_U(s)$, $M_V(s)$, and $M_{UV}(s)$ are the corresponding MGFs of $F_U(x)$, $F_V(x)$ and $F_U(x)F_V(x)$, respectively.

From (5) and (6) we can see that, U has the identical statistical characteristics as γ_{sd}, either the CDF or the MGF. In this case, the derivation can be simplified. Thus, similar to (22) we have

$$M_U(s)=\frac{\left(\frac{\bar{\gamma}_b\Omega_{\mathrm{br}}}{m_{\mathrm{br}}\bar{\gamma}_{\mathrm{th}}}\right)^{\tilde{\varphi}_{\mathrm{sr}}}}{\Gamma\left(m_{\mathrm{br}}\right)Q_2}s^{-\tilde{\varphi}_{\mathrm{sr}}}G_{42}^{24}\left[\frac{b_{\mathrm{sr}}^2\bar{\gamma}_{\mathrm{b}}\Omega_{\mathrm{br}}}{s\bar{\gamma}_{\mathrm{th}}b_{\mathrm{sc}}^2 m_{\mathrm{br}}}\,\middle|\,\begin{array}{c} 1-\tilde{\varphi}_{\mathrm{sr}},1-m_{\mathrm{br}}-\tilde{\varphi}_{\mathrm{sr}},1-\varphi_{\mathrm{sc}}-\tilde{\varphi}_{\mathrm{sr}},1-\varepsilon_{\mathrm{sc}}-\tilde{\varphi}_{\mathrm{sr}} \\ \tilde{\varepsilon}_{\mathrm{sr}},-\tilde{\varepsilon}_{\mathrm{sr}} \end{array}\right],\tag{25}$$

where $Q_2=\Gamma(\varepsilon_{\mathrm{sc}})\Gamma(\varphi_{\mathrm{sc}})\Gamma(\varepsilon_{\mathrm{sr}})\Gamma(\varphi_{\mathrm{sr}})$.

Next, we concentrate on deriving $M_V(s)$. From $V = \frac{\bar{\gamma}_{\text{th}} Y}{\bar{\gamma}_{\text{b}} |h_{\text{bd}}|^2 + 1}$ with $Y = \frac{|h_{\text{rd}}|^2}{|h_{\text{rc}}|^2}$, $F_V(x)$ can be calculated as

$$F_V(x) = \int_0^\infty f_{\bar{\gamma}_{\text{b}} |h_{\text{bd}}|^2}(y) F_{\bar{\gamma}_{\text{th}} Y}(xy) \mathrm{d}y, \tag{26}$$

where $F_Y(x)$ can be written as

$$F_Y(x) = \int_0^\infty F_{|h_{\text{rd}}|^2}(xy) f_{|h_{\text{rd}}|^2}(y) \mathrm{d}y. \tag{27}$$

From (8) we can get $F_{|h_{\text{rd}}|^2}(x) = \Upsilon(m_{\text{rd}}, \frac{m_{\text{rd}}}{\Omega_{\text{rd}}} x)/\Gamma(m_{\text{rd}})$, where $\Upsilon(\alpha, x)$ denotes the lower incomplete Gamma function [27, Eq. (8.350.1)]. Then, $F_Y(x)$ can be obtained as

$$F_Y(x) = \frac{m_{\text{rc}}^{m_{\text{rc}}}}{\Gamma(m_{\text{rd}}) \Gamma(m_{\text{rc}}) \Omega_{\text{rc}}^{m_{\text{rc}}}} \int_0^\infty y^{m_{\text{rc}}-1} \mathrm{e}^{-\frac{m_{\text{rc}}}{\Omega_{\text{rc}}} y} \Upsilon\left(m_{\text{rd}}, \frac{m_{\text{rd}}}{\Omega_{\text{rd}}} xy\right) \mathrm{d}y. \tag{28}$$

Using [27, Eq. (6.455.2)], we can obtain

$$F_Y(x) = \frac{m_{\text{rc}}^{m_{\text{rc}}} m_{\text{rd}}^{m_{\text{rd}}-1}}{B(m_{\text{rd}}, m_{\text{rc}}) \Omega_{\text{rc}}^{m_{\text{rc}}} \Omega_{\text{rd}}^{m_{\text{rd}}}} \left(\frac{m_{\text{rd}}}{\Omega_{\text{rd}}} x + \frac{m_{\text{rc}}}{\Omega_{\text{rc}}}\right)^{-m_{\text{rd}}-m_{\text{rc}}} {}_2F_1\left(1, m_{\text{rd}}+m_{\text{rc}}; m_{\text{rd}}+1; \frac{\frac{m_{\text{rd}}}{\Omega_{\text{rd}}} x}{\frac{m_{\text{rd}}}{\Omega_{\text{rd}}} x + \frac{m_{\text{rc}}}{\Omega_{\text{rc}}}}\right), \tag{29}$$

where $B(m, n) = \frac{\Gamma(m)\Gamma(n)}{\Gamma(m+n)}$ denotes the Beta function [27, Eq. (8.384.1)]. For the convenience of subsequent derivation, we express the Gauss Hypergeometric function ${}_2F_1(a, b; c; z)$ as the sum of L terms [27, Eq. (9.100)]. Then, we can get

$$F_V(x) = \frac{m_{\text{bd}}^{m_{\text{bd}}} m_{\text{rc}}^{m_{\text{rc}}}}{\Gamma(m_{\text{bd}}) B(m_{\text{rd}}, m_{\text{rc}}) (\bar{\gamma}_{\text{b}}\Omega_{\text{bd}})^{m_{\text{bd}}} \Omega_{\text{rc}}^{m_{\text{rc}}}} \sum_{p=0}^L \frac{(1)_p (m_{\text{rd}}+m_{\text{rc}})_p m_{\text{rd}}^{p+m_{\text{rd}}-1}}{(m_{\text{rd}}+1)_p p! \Omega_{\text{rd}}^{p+m_{\text{rd}}} \bar{\gamma}_{\text{th}}^{p+1}} x^p$$
$$\times \int_0^\infty y^{m_{\text{bd}}+p-1} \mathrm{e}^{-\frac{m_{\text{bd}}}{\bar{\gamma}_{\text{b}}\Omega_{\text{bd}}} y} \left(\frac{m_{\text{rd}}}{\Omega_{\text{rd}}\bar{\gamma}_{\text{th}}} xy + \frac{m_{\text{rc}}}{\Omega_{\text{rc}}}\right)^{-\tilde{p}} \mathrm{d}y, \tag{30}$$

where $(u)_v = \Gamma(u+v)/\Gamma(u)$ denotes the Pochhammer symbol and $\tilde{p} = p + m_{\text{rd}} + m_{\text{rc}}$. To solve the integral, we express $(\frac{m_{\text{rd}}}{\Omega_{\text{rd}}\bar{\gamma}_{\text{th}}} xy + \frac{m_{\text{rc}}}{\Omega_{\text{rc}}})^{-\tilde{p}}$ into Meijer-G function with the aid of [30, Eq. (10)], i.e.,

$$\left(\frac{m_{\text{rd}}}{\Omega_{\text{rd}}\bar{\gamma}_{\text{th}}} xy + \frac{m_{\text{rc}}}{\Omega_{\text{rc}}}\right)^{-\tilde{p}} = \frac{(\frac{m_{\text{rc}}}{\Omega_{\text{rc}}})^{-\tilde{p}}}{\Gamma(\tilde{p})} G_{11}^{11}\left[\frac{m_{\text{rd}}\Omega_{\text{rc}} x}{\Omega_{\text{rd}}\bar{\gamma}_{\text{th}} m_{\text{rc}}} y \,\middle|\, \begin{matrix} 1-\tilde{p} \\ 0 \end{matrix}\right]. \tag{31}$$

Substituting (31) into (30) and employing [27, Eq. (7.813.1)], $F_V(x)$ can be derived as

$$F_V(x) = A_3 x^p G_{21}^{12}\left[\frac{m_{\text{rd}}\Omega_{\text{rc}}\Omega_{\text{bd}}\bar{\gamma}_b}{m_{\text{bd}} m_{\text{rc}}\Omega_{\text{rd}}\bar{\gamma}_{\text{th}}} x \,\middle|\, \begin{matrix} 1-m_{\text{bd}}-p, 1-\tilde{p} \\ 0 \end{matrix}\right], \tag{32}$$

where $A_3 = \frac{1}{\Gamma(m_{\text{bd}}) B(m_{\text{rd}}, m_{\text{rc}}) m_{\text{rd}}} \sum_{p=0}^L \frac{(1)_p (m_{\text{rd}}+m_{\text{rc}})_p}{(m_{\text{rd}}+1)_p p! \Gamma(\tilde{p})} (\frac{m_{\text{bd}}}{\bar{\gamma}_{\text{b}}\Omega_{\text{bd}}})^{-p} (\frac{m_{\text{rd}}\Omega_{\text{rc}}}{\Omega_{\text{rd}} m_{\text{rc}}})^{p+m_{\text{rd}}} \frac{1}{\bar{\gamma}_{\text{th}}^{p+1}}$. Then, $M_V(s)$ can be derived as

$$M_V(s) = \int_0^\infty s\mathrm{e}^{-sx} F_V(x) \mathrm{d}x = A_3 s^{-p} G_{31}^{13}\left[\frac{m_{\text{rd}}\Omega_{\text{rc}}\Omega_{\text{bd}}\bar{\gamma}_b}{m_{\text{bd}} m_{\text{rc}}\Omega_{\text{rd}}\bar{\gamma}_{\text{th}} s} \,\middle|\, \begin{matrix} -p, 1-m_{\text{bd}}-p, 1-\tilde{p} \\ 0 \end{matrix}\right]. \tag{33}$$

Finally, $M_{UV}(s)$ can be calculated as

$$M_{UV}(s) = \int_0^\infty s\mathrm{e}^{-sx} F_U(x) F_V(x) \mathrm{d}x. \tag{34}$$

By expanding e^{-sx} into series with L terms and using the equality in [27, Eq. (7.811.1)], we can derive $M_{UV}(s)$ as

$$M_{UV}(s) = A_4 s^{k+1}, \tag{35}$$

Table 1 Channel parameters for generalized-K fading [25]

Shadowing	σ	φ_i	ε_i
Infrequent light shadowing (ILS)	0.115	75.1155	3
Average shadowing (AS)	0.345	7.9115	2
Frequent heavy shadowing (FHS)	0.806	1.0931	1

where

$$
A_4 = A_3 \frac{\left(\frac{\bar{\gamma}_{\mathrm{b}}\Omega_{\mathrm{br}}}{m_{\mathrm{br}}\bar{\gamma}_{\mathrm{th}}}\right)^{\tilde{\varphi}_{\mathrm{sr}}}}{\Gamma\left(m_{\mathrm{br}}\right) Q_2} \sum_{k=0}^{L} \frac{(-1)^k}{k!} \left(\frac{b_{\mathrm{sr}}^2 \bar{\gamma}_{\mathrm{b}}\Omega_{\mathrm{br}}}{\bar{\gamma}_{\mathrm{th}} b_{\mathrm{sc}}^2 m_{\mathrm{br}}}\right)^{-\tilde{k}-\tilde{\varphi}_{\mathrm{sr}}-1}
$$

$$
\cdot G_{55}^{54}\left[\frac{m_{\mathrm{rd}}m_{\mathrm{br}}\Omega_{\mathrm{rc}}\Omega_{\mathrm{bd}}b_{\mathrm{sc}}^2}{m_{\mathrm{bd}}m_{\mathrm{rc}}\Omega_{\mathrm{rd}}\Omega_{\mathrm{br}}b_{\mathrm{sr}}^2} \,\middle|\, \begin{array}{c} 1-p-m_{\mathrm{bd}}, 1-\tilde{p}, -\tilde{k}-\varphi_{\mathrm{sr}}, -\tilde{k}-\varepsilon_{\mathrm{sr}}, -\tilde{k} \\ 0, -\tilde{k}-2\tilde{\varphi}_{\mathrm{sr}}-1, m_{\mathrm{br}}-\tilde{k}-1, \varphi_{\mathrm{sc}}-\tilde{k}-1, \varepsilon_{\mathrm{sc}}-\tilde{k}-1 \end{array}\right]
$$

with $\tilde{k}=p+k$. Combining the derived (25), (33), and (35), we can obtain a closed-form expression for $M_{\gamma_{\mathrm{srd}}}(s)$.

Until now, we have obtained the closed-form expression for $M_{\gamma_{\mathrm{coop}}}(s)$ based on the expressions of $M_{\gamma_{\mathrm{sd}}}(s)$ and $M_{\gamma_{\mathrm{srd}}}(s)$. Subsequently, in the derivation of average SER, considering there is no closed-form solution for the integral in (9), we employ the tight approximate expression in [32, Eq. (30)] to obtain $\mathcal{P}_{\mathrm{ser}}$. While in the derivation of $\mathcal{P}_{\mathrm{out}}$, we substitute $M_{\gamma_{\mathrm{coop}}}(s)$ into (10) directly.

4 Results and analysis

In this section, we conduct simulations to demonstrate the validity of the theoretical analysis and investigate how the system parameters affect the performance of the CSTCN. In this network, satellite downlinks are all modeled as generalized-K distributions with $\Omega_i = 1$. The detailed channel parameters are given in Table 1, where σ is the standard deviation of the log-normal shadowing and increases as the amount of fading increases. According to [25], φ_i of the generalized-K distribution can be expressed as $\varphi_i = \frac{1}{e^{\sigma^2}-1}$. In practical applications, the relay node is usually placed at a higher position than the destination node, which results in that S $\rightarrow$ R link usually undergoes a more light shadowing than S $\rightarrow$ D link. Thus, we consider three shadowing cases for satellite communications. In the first case, we assume S $\rightarrow$ R and S $\rightarrow$ D channels undergo infrequent light shadowing and average shadowing, referred to as ILS-AS ($\sigma_{\mathrm{sr}} = 0.115, \sigma_{\mathrm{sd}} = 0.345$). Similarly, ILS-FHS ($\sigma_{\mathrm{sr}} = 0.115, \sigma_{\mathrm{sd}} = 0.806$) for the second case and AS-FHS ($\sigma_{\mathrm{sr}} = 0.345, \sigma_{\mathrm{sd}} = 0.806$) for the third case. Moreover, we set $m_{\mathrm{br}} = m_{\mathrm{bd}} = m_{\mathrm{rc}} = 2$ and $\Theta_{\mathrm{th}} = 3$ dB.

Figures 2 and 3 firstly show the SER and OP versus the threshold-to-noise ratio $\bar{\gamma}_{\mathrm{th}}$, respectively, where communication links experience various shadowing cases. As expected, as the interference constraint imposed by terrestrial communications gets looser, we can achieve a better SER performance. For various shadowing cases of h_{sr} and h_{sd} under a given m_{rd}, the SER performance with ILS-AS fading outperforms that with ILS-FHS fading and finally the AS-FHS fading. Moreover, as m_{rd} increases which indicates a better communication quality of the R-D link, we can achieve a much reliable communication. Furthermore, the theoretical results obtained from (9) and (10) agree well with the simulation results, verifying the validity of our theoretical analysis.

Figure 4 illustrates the effect of the interference from the licensed terrestrial system on the SER performance of the secondary satellite communication with different modulation constellations. As observed, the SER increases as the BS transmit power-to-noise ratio $\bar{\gamma}_{\mathrm{b}}$ gradually increases from 0 to 15 dB. It is interesting to note that for a given modulation constellation, the curves with different $\bar{\gamma}_{\mathrm{b}}$ are parallel with each other at high SNR region. This phenomenon reveals that the co-channel interference caused by spectrum sharing can only degrades the SER performance, while the diversity order introduced by co-
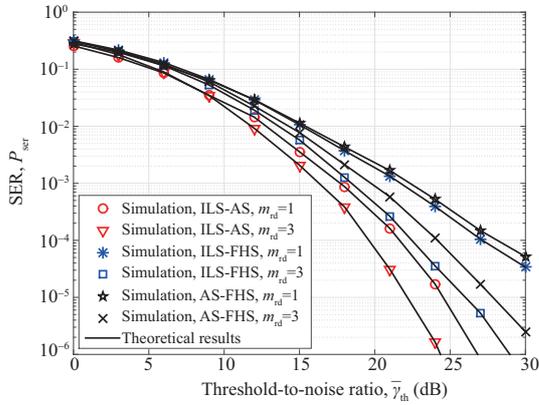
Figure 2 (Color online) SER versus $\bar{\gamma}_{\mathrm{th}}$ with QPSK for various shadowing cases ($\bar{\gamma}_{\mathrm{b}} = 2$ dB).
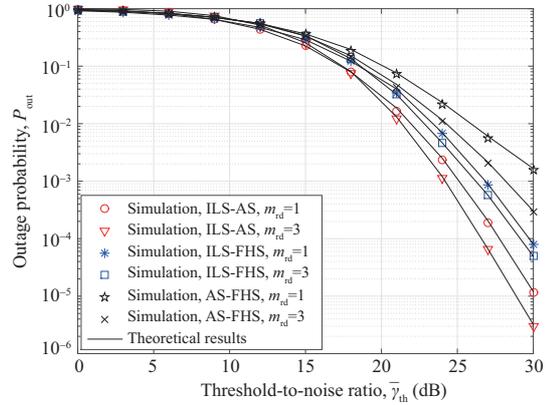
Figure 3 (Color online) OP versus $\bar{\gamma}_{\mathrm{th}}$ for various shadowing cases ($\bar{\gamma}_{\mathrm{b}} = 2$ dB).
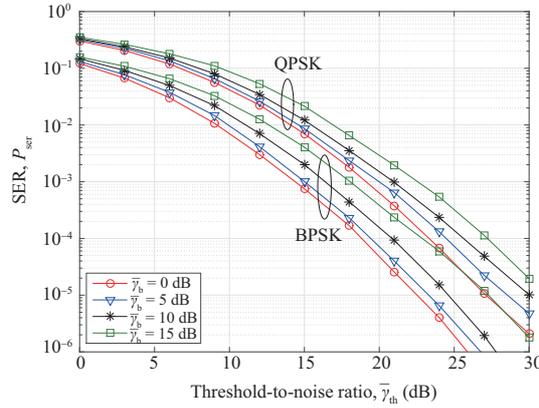
Figure 4 (Color online) SER versus $\bar{\gamma}_{\mathrm{th}}$ for various $\bar{\gamma}_{\mathrm{b}}$ with AS-FHS shadowing case ($m_{\mathrm{rd}} = 3$).
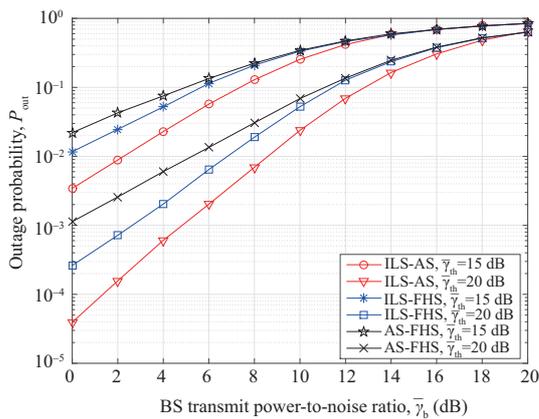
Figure 5 (Color online) OP versus $\bar{\gamma}_{\mathrm{b}}$ for various $\bar{\gamma}_{\mathrm{th}}$ and shadowing cases ($m_{\mathrm{rd}} = 3$).
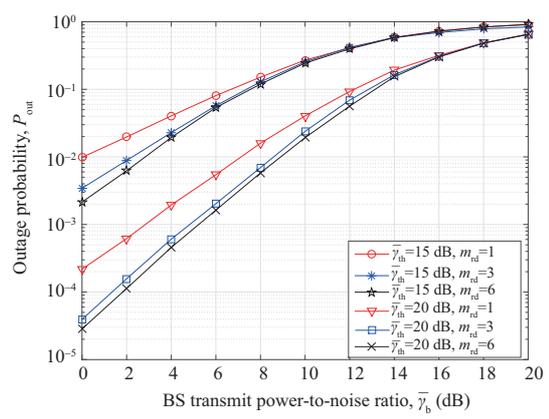
Figure 6 (Color online) OP versus $\bar{\gamma}_{\mathrm{b}}$ for various $\bar{\gamma}_{\mathrm{th}}$ and m_{rd} with ILS-AS shadowing.

operative communication can be maintained. Moreover, the SER performance under BPSK modulation is superior to that with QPSK modulation.

Figures 5 and 6 depict the OP versus $\bar{\gamma}_{\mathrm{b}}$ for various m_{rd}, threshold-to-noise ratios $\bar{\gamma}_{\mathrm{th}}$, and shadowing cases. From both figures we can see that the OP gets larger when either the $\bar{\gamma}_{\mathrm{b}}$ increases, or the $\bar{\gamma}_{\mathrm{th}}$ decreases, or the shadowing becomes severer, all of which would result in a lower SINR at the destination.

Moreover, the curves with different shadowing cases coincide with each other eventually, which indicates when $\bar{\gamma}_{\rm b}$ is large, the inter-system interference will dominate the received SINR no matter what shadowing the desired signal experiences. Besides, it can be observed that as $m_{\rm rd}$ increases from 1 to 6, the gaps between the corresponding OP curves become smaller, which reveals when the relay-destination link experiences mild fading, the outage performance is mainly subject to the shadowing of satellite downlinks.

5   Conclusions

In this paper, we have evaluated the performance of the underlay CSTCN in terms of SER and OP. Taking the inter-system interference into account, we restrict the transmit power of satellite communications by the interference power constraints while consider both the relay and destination receiving interference from cellular communications. Based on the MGF approach, closed-form expressions for the SER and OP have been obtained. Simulations have confirmed the accuracy of the obtained theoretical results, and shown the impact of shadowing case, interference power constrain, and other vital system parameters on network performance.

References

1   Evans B, Werner M, Lutz E, et al. Integration of satellite and terrestrial systems in future multimedia communications. IEEE Wirel Commun, 2005, 12: 72–80
2   Sadek M, Aissa S. Personal satellite communication: technologies and challenges. IEEE Wirel Commun, 2012, 19: 28–35
3   Ruan Y H, Li Y Z, Wang C X, et al. Energy efficient adaptive transmissions in integrated satellite-terrestrial networks with SER constraints. IEEE Trans Wirel Commun, 2018, 17: 210–222
4   Li H J, Yin H, Dong F H, et al. Capacity upper bound analysis of the hybrid satellite terrestrial communication systems. IEEE Commun Lett, 2016, 20: 2402–2405
5   Zhang J X, Evans B, Imran M A, et al. Green hybrid satellite terrestrial networks: fundamental trade-off analysis. In: Proceedings of IEEE Vehicular Technology Conference (VTC'16), Nanjing, 2016
6   Arti M K, Jindal S K. OSTBC transmission in shadowed-Rician land mobile satellite links. IEEE Trans Veh Technol, 2016, 65: 5771–5777
7   Khan A H, Imran M A, Evans B G. Semi-adaptive beamforming for OFDM based hybrid terrestrial-satellite mobile system. IEEE Trans Wirel Commun, 2012, 11: 3424–3433
8   Sithamparanathan K, de Nardis L, Di Benedetto M G, et al. Cognitive satellite terrestrial radios. In: Proceedings of IEEE Global Communications Conference (GLOBECOM'10), Miami, 2010
9   Ge X H, Tu S, Mao G Q, et al. 5G ultra-dense cellular networks. IEEE Wirel Commun, 2016, 23: 72–79
10   Wang C X, Wu S B, Bai L, et al. Recent advances and future challenges for massive MIMO channel measurements and models. Sci China Inf Sci, 2016, 59: 021301
11   Höyhtyä M, kyröläinen J, Hulkkonen A, et al. Application of cognitive radio techniques to satellite communication. In: Proceedings of IEEE International Symposium on Dynamic Spectrum Access Networks (DYSPAN'12), Bellevue, 2012. 540–551
12   Sharma S K, Chatzinotas S, Ottersten B. Satellite cognitive communications: interference modeling and techniques selection. In: Proceedings of IEEE Advanced Satellite Multimedia Systems Conference (ASMS) and Signal Processing for Space Communications Workshop (SPSC), Baiona, 2012. 111–118
13   Haider F, Wang C X, Haas H, et al. Spectral and energy efficiency analysis for cognitive radio networks. IEEE Trans Wirel Commun, 2015, 14: 2969–2980
14   Icolari V, Guidotti A, Tarchi D, et al. An interference estimation technique for satellite cognitive radio systems. In: Proceedings of IEEE International Conference on Communications (ICC'15), London, 2015. 892–897
15   Kuang L L, Chen X, Jiang C X, et al. Radio resource management in future terrestrial-satellite communication networks. IEEE Wirel Commun, 2017, 24: 81–87
16   Ruan Y H, Li Y Z, Wang C X, et al. Outage performance of integrated satellite-terrestrial networks with hybrid CCI. IEEE Commun Lett, 2017, 21: 1545–1548

17 Lagunas E, Sharma S K, Maleki S, et al. Resource allocation for cognitive satellite communications with incumbent terrestrial networks. IEEE Trans Cogn Commun Netw, 2015, 1: 305–317

18 Guidolin F, Nekovee M, Badia L, et al. A cooperative scheduling algorithm for the coexistence of fixed satellite services and 5G cellular network. In: Proceedings of IEEE International Conference on Communications (ICC'15), London, 2015. 1322–1327

19 Zhang W S, Wang C X, Chen D, et al. Energy-spectral efficiency tradeoff in cognitive radio networks. IEEE Trans Veh Technol, 2016, 65: 2208–2218

20 An K, Ouyang J, Lin M, et al. Outage analysis of multi-antenna cognitive hybrid satellite-terrestrial relay networks with beamforming. IEEE Commun Lett, 2015, 19: 1157–1160

21 Bhatnagar M R, Arti M K. Performance analysis of AF based hybrid satellite-terrestrial cooperative network over generalized fading channels. IEEE Commun Lett, 2013, 17: 1912–1915

22 Sreng S, Escrig B, Boucheret M L. Exact symbol error probability of hybrid/integrated satellite-terrestrial cooperative network. IEEE Trans Wirel Commun, 2013, 12: 1310–1319

23 Ruan Y H, Li Y Z, Zhang R, et al. Performance analysis of hybrid satellite-terrestrial cooperative networks with distributed alamouti code. In: Proceedings of IEEE Vehicular Technology Conference (VTC'16), Nanjing, 2016

24 Chun L. A statistical model for a land mobile satellite link. IEEE Trans Veh Technol, 1985, 34: 122–127

25 Peppas K P. Accurate closed-form approximations to generalised-K sum distributions and applications in the performance analysis of equal-gain combining receivers. IET Commun, 2011, 5: 982–989

26 Ruan Y H, Li Y Z, Wang C X, et al. Effective capacity analysis for underlay cognitive satellite-terrestrial networks. In: Proceedings of IEEE International Conference on Communications (ICC'17), Paris, 2017

27 Gradshteyn I S, Ryzhik I M. Table of Integrals, Series, and Products. 6th ed. Orlando: Academic Press, 2000

28 Simon M K, Alouini M S. Digital Communication over Fading Channels. Hoboken: John Wiley & Sons, 2005

29 Simon M K, Alouini M S, Ko Y C. Outage probability of diversity systems over generalized fading channels. IEEE Trans Commun, 2000, 48: 1783–1787

30 Adamchik V S, Marichev O I. The algorithm for calculating integrals of hypergeometric type functions and its realization in reduce systems. In: Proceedings of International Conference Symposium on Algebraic Computing, Tokyo, 1990. 212–224

31 Ikki S S, Aissa S. Performance analysis of two-way amplify-and-forward relaying in the presence of co-channel interferences. IEEE Trans Commun, 2012, 60: 933–939

32 Mckay M R, Zanella A, Collings I B, et al. Error probability and SINR analysis of optimum combining in rician fading. IEEE Trans Commun, 2009, 57: 676–687